PHYSICAL REVIEW B **72**, 100101(R) (2005)

Dislocation formation and plastic flow in binary alloys in three dimensions

Akihiko Minami and Akira Onuki
Department of Physics, Kyoto University, Kyoto 606-8502, Japan
(Received 28 April 2005; published 6 September 2005)

We develop a nonlinear elasticity theory in which the elastic energy is a periodic function of five strain components in three dimensions. We then study dislocation formation under applied shear strain in one and two phase alloys. In two phase states loops of edge dislocations appear in the interface regions with increasing strain. They grow into the softer regions gliding along the Burgers vector. These results are crucial to understand mechanical properties of two phase solids.

DOI: 10.1103/PhysRevB.72.100101 PACS number(s): 62.20.Fe, 64.70.Kb, 81.40.Cd

Dislocations often play decisive roles in various phase transformations in crystalline solids. They are produced when the lattice constants or the crystalline structures of the two phases are not close.[1] With their appearance the continuity of the lattice planes through the interfaces is lost partially or even completely, resulting in the so-called coherency loss. In particular, coarsening of incoherent microstructures has been studied in fcc Al-Sc alloys.[2] It is also known that dislocations are proliferated in plastic flow. In two phase states such dislocations grow into the softer regions with their ends pinned at the interfaces.[3,4] As a result, mechanical properties of two phase solids are very different from those of one phase solids.[1]

Most theoretical papers on the elastic effects in phase transitions have treated the coherent case without dislocations.[5–8] Theory in the incoherent case is much more difficult and numerical studies have been performed in two dimensions (2D)[9–11] and in three dimensions (3D).[12] In these simulations dislocations have been treated as singular points or lines in the linear elasticity scheme. Though in 2D, we recently presented numerical results of dislocation formation and gliding in two phase solids[13] on the basis of a simple nonlinear elasticity theory.[14] In 3D, however, dislocations are mobile curved lines and assume very complex configurations and 3D simulations are needed to understand the real physical processes.[15,16] In this Rapid Communication we will develop a 3D nonlinear elasticity theory, perform 3D simulations both in one and two phase states, and provide physical pictures of these complex phenomena. A merit of our approach is its extreme simplicity, while it still captures the realistic dislocation dynamics.

We consider an AB alloy without vacancies and interstitials, where the order parameter ψ is the composition difference in the range $-1 \leqq \psi \leqq 1$. In the free energy $F=\int d\boldsymbol{r} f$, ψ is coupled to the elastic displacement $\boldsymbol{u}=(u_x,u_y,u_z)$. The free energy density f is written as

$$f=\frac{k_B}{v_0}\left[T\frac{1+\psi}{2}\ln(1+\psi)+T\frac{1-\psi}{2}\ln(1-\psi)-\frac{T_0}{2}\psi^2\right] + \frac{1}{2}C|\nabla\psi|^2+\alpha\psi e_1+f_{\rm el}(\boldsymbol{u},\psi). \quad (1)$$

The first term is the Bragg-Williams free energy density where v_0 is the volume of a unit cell, T_0 is the critical temperature in the absence of the elastic coupling. The second term is the gradient term. The third term is the coupling between ψ and the dilation strain $e_1=\nabla\cdot\boldsymbol{u}$ arising from the atomic size difference of the two components.[5] The last term is the elastic free energy,

$$f_{\rm el}=\frac{1}{2}Ke_1^2+\Phi(e_2,e_3)+\Psi(e_4,e_5,e_6). \quad (2)$$

Supposing a cubic solid with the principal axes in the x, y, and z directions, we define the strain components as

$$e_2=\epsilon_{xx}-\epsilon_{yy}, \quad e_3=(2\epsilon_{zz}-\epsilon_{xx}-\epsilon_{yy})/\sqrt{3},$$

$$e_4=\epsilon_{xy}, \quad e_5=\epsilon_{yz}, \quad e_6=\epsilon_{zx}, \quad (3)$$

where $\epsilon_{ij}=(\partial u_i/\partial x_j+\partial u_j/\partial x_i)/2$. The diagonal strains e_2 and e_3 give rise to a contribution due to stretching,

$$\Phi=\frac{\mu_2}{4\pi^2}\left[3-\cos(2\pi e_{2-})-\cos(2\pi e_{2+})-\cos\left(\frac{4\pi}{\sqrt{6}}e_3\right)\right], \quad (4)$$

where $e_{2\pm}=e_2/\sqrt{2}\pm e_3/\sqrt{6}$. The shear strains e_4, e_5, and e_6 give rise to a shear contribution,

$$\Psi=\frac{\mu_3}{4\pi^2}[3-\cos(2\pi e_4)-\cos(2\pi e_5)-\cos(2\pi e_6)]. \quad (5)$$

Notice that Φ and Ψ are invariant with respect to a $\pi/2$ rotation around the x axis, which changes the strains as $e_2'=e_2/2-\sqrt{3}e_3/2$, $e_3'=-\sqrt{3}e_2/2-e_3/2$, $e_4'=e_6$, $e_5'=-e_5$, and $e_6'=-e_4$. Similarly, they are invariant with respect to $\pi/2$ rotations around the y and z axes.[17] For small strains we obtain the standard forms, $\Phi\cong\mu_2(e_2^2+e_3^2)/2$ and $\Psi\cong\mu_3(e_4^2+e_5^2+e_6^2)/2$, in the linear elasticity theory.[18] The crystal is also unchanged with respect to shear deformation $u_x\to u_x+y$ or $e_4\to e_4+1$ in the xy plane. Thus $f_{\rm el}$ is required to be a periodic function of e_4, e_5 and e_6 with period 1. The simplest elastic energy satisfying these requirements is given by Eq. (2). The elastic moduli μ_2 and μ_3 depend on ψ as[8]

$$\mu_2=\mu_{20}+\mu_{21}\psi, \quad \mu_3=\mu_{30}+\mu_{31}\psi, \quad (6)$$

while the bulk modulus K is a constant. For positive μ_{20} and μ_{30} the regions with larger (smaller) ψ are harder (softer) than those with smaller (larger) ψ. It is known that aniso-

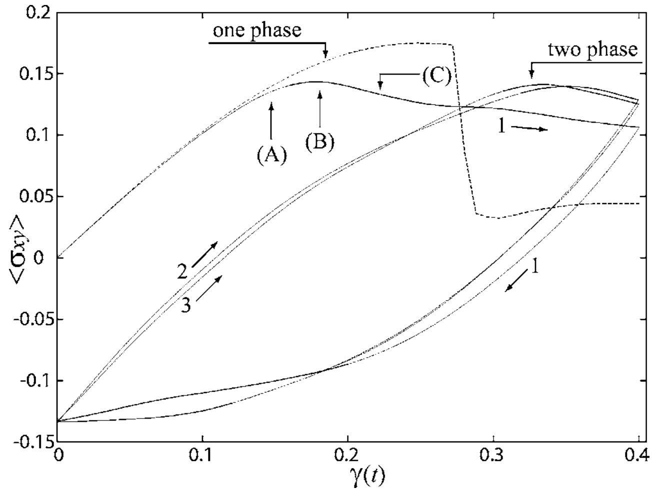

FIG. 1. Stress vs strain in a one phase state (broken line) and in a two phase state under cyclic shear (solid line). There are no defects initially. Edge dislocations appear in plastic flow.

tropic elastic deformations tend to be localized in the softer regions in phase separation.[8]

The lattice velocity $\boldsymbol{v}=\partial \boldsymbol{u}/\partial t$ obeys

$$\rho\frac{\partial \boldsymbol{v}}{\partial t}=\nabla\cdot\overleftrightarrow{\sigma}+\eta_0\nabla^2\boldsymbol{v}, \tag{7}$$

where ρ is the mass density and $\overleftrightarrow{\sigma}=\{\sigma_{ij}\}$ is the elastic stress tensor $(=\partial f/\partial\epsilon_{ij})$. For example, $\sigma_{xy}=\mu_3\sin(2\pi e_4)/2\pi$. The nonlinearity of $\overleftrightarrow{\sigma}$ is most important in Eq. (7). We introduce the shear viscosity η_0, which gives rise to damping of $\boldsymbol{u}$. The composition is governed by the diffusive equation

$$\frac{\partial\psi}{\partial t}=\nabla\cdot\lambda(\psi)\nabla\frac{\delta}{\delta\psi}F. \tag{8}$$

The kinetic coefficient is assumed to be of the form $\lambda(\psi)=\lambda_0(1-\psi^2)$. Then ψ obeys a simple diffusion equation in the

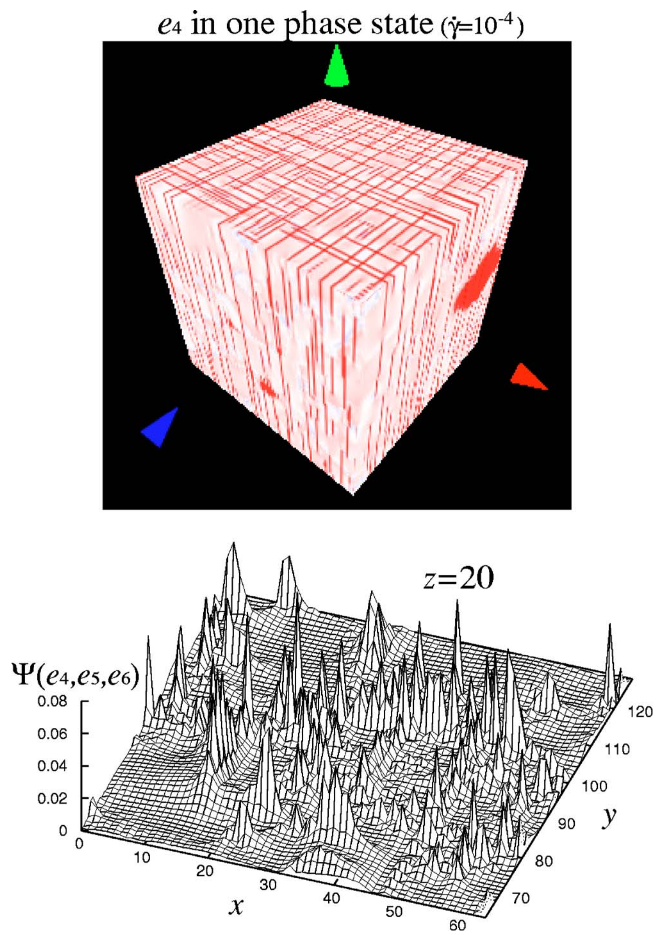

FIG. 2. (Color online) Shear strain e_4 exhibiting slip planes (upper plate) and shear deformation energy Ψ at $z=20$ with peaks at dislocation cores (lower plate) in a one phase state at $\gamma=0.296$. A 1/4 of the total plane is shown in the lower figure. The x, y, and z axes are in red, blue, and green, respectively.

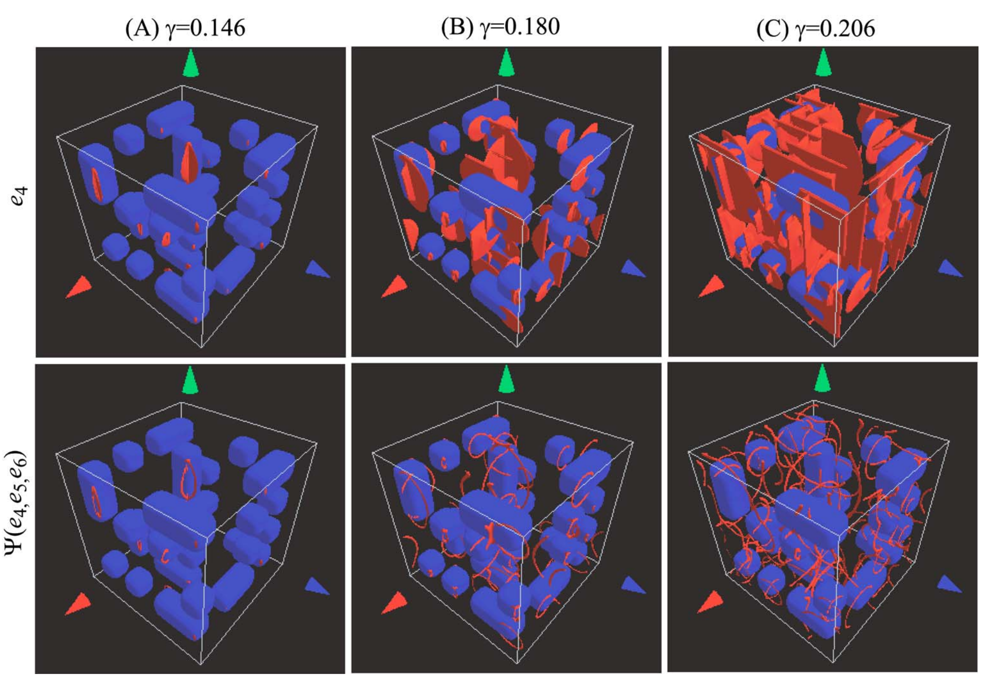

FIG. 3. (Color online) Time evolution of e_4 (upper figures) and Ψ (lower figures) under shear $\gamma=\dot{\gamma}t$. They take large values on slip planes and dislocation cores, respectively. Blue regions represent hard domains. Dislocation loops are trapped at the interfaces.

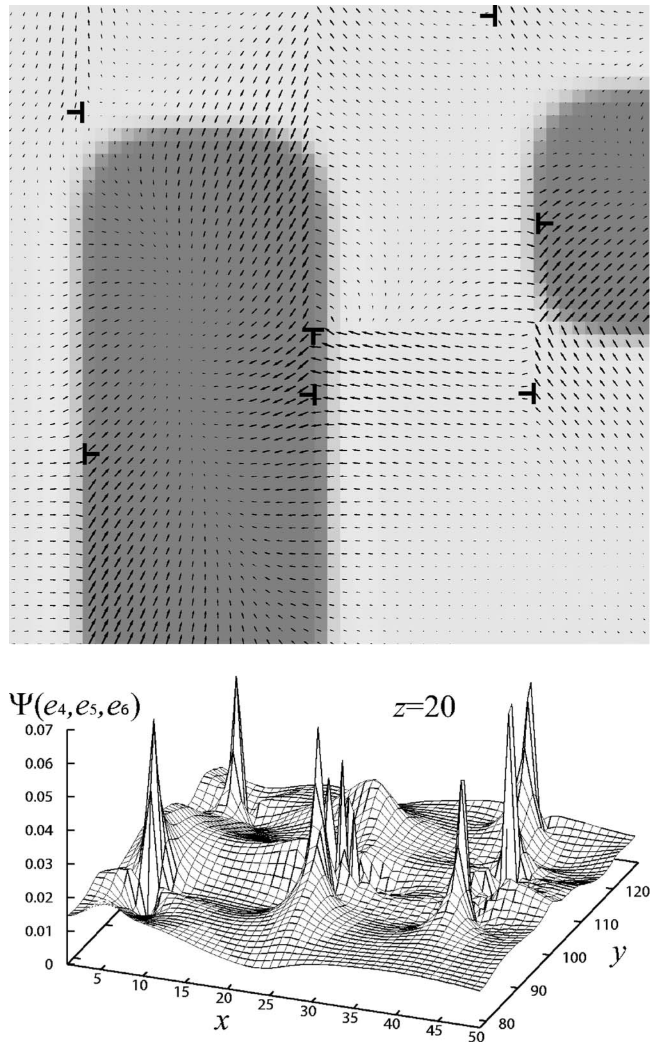

FIG. 4. Displacement deviation $(u_x-\gamma y, u_y)$ (upper plate) and Ψ (lower plate) at $\gamma=0.206$ on a $1/4$ plane at $z=20$. The $\perp$ (indicating the Burgers vector) in the upper figure and the peaks in the lower figure represent edge dislocations.

dilute limit $\psi\rightarrow\pm1$ with the diffusion constant $D_0=\lambda_0 k_B T/v_0$. Without applied stress, Eqs. (7) and (8) yield $dF_T/dt \leqq 0$ assuring approach to equilibrium, where $F_T=F+\int d\boldsymbol{r}\rho\boldsymbol{v}^2/2$ is the total free energy. In this sence they are self-consistent.[19]

We numerically integrated Eqs. (7) and (8) on a $128\times128\times128$ lattice using a staggered lattice method.[14] The mesh size is equal to the lattice constant a. We applied average shear strain $\gamma=\langle\partial u_x/\partial y\rangle=\langle e_4\rangle$ and imposed the periodic boundary condition on the deviation $\delta\boldsymbol{u}=(u_x-\gamma y, u_y, u_z)$. We set $K/\mu_{20}=4.5$, $\alpha/\mu_{20}=1.5$, and $k_B T_0/v_0\mu_{20}=0.05$ in terms of μ_{20} in Eq. (6). Space, time, and temperature will be measured in units of a, $\tau_0=a(\rho/\mu_{20})^{1/2}$, and $v_0\mu_{20}/k_B$. We assume weak cubic elastic anisotropy with $\mu_{30}/\mu_{20}=1.1$ and moderate elastic inhomogeneity with $\mu_{21}=\mu_{31}=0.6\mu_{20}$. The spinodal temperature, below which one phase states become unstable, is then $T_s\cong0.43$ at $\langle\psi\rangle=0$. The dimensionless kinetic coefficients are $\lambda^*=\lambda_0\tau_0\mu_{20}a^{-2}=10^{-4}$ and $\eta^*=\eta_0/\tau_0\mu_{20}=0.1$. The relaxation of $\boldsymbol{u}$ is faster than that

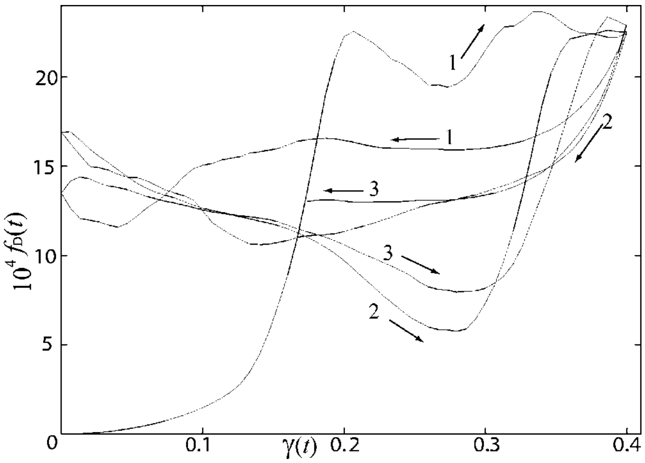

FIG. 5. Defect energy density $f_D(t)$ defined by Eq. (9) in units of μ_{20} vs strain $\gamma(t)$ in cyclic shear in a two phase state.

of ψ by $\eta^*/\lambda^*=\eta_0/D_0\rho=10^3$, so we integrated Eq. (7) using an implicit Crank-Nicolson method. In Fig. 1 we show the average stress $\langle\sigma_{xy}\rangle$ in units of μ_{20} after application of shear at $t=0$. The shear rate $\dot{\gamma}=d\gamma/dt$ will be measured in units of τ_0^{-1}.

In the one phase case we set $T\cong0.5$ and $\dot{\gamma}=10^{-4}$.[20] The initial value of $\boldsymbol{u}$ is a random Gaussian number with variance $0.01a$ at each lattice point. The stress exhibits a sharp overshoot with appearance of edge dislocations. In our case the instability point of homogeneous states is given by $\partial^2\Psi/\partial e_4^2=\mu_3\cos(2\pi e_4)=0$ or $\gamma=e_4=1/4$. Figure 2 displays a 3D snapshot of the shear strain e_4 and a 2D cross section of the shear elastic energy Ψ at $z=20$ for $\gamma=0.296$. We can see multiple formation of slip planes (upper plate) and edge dislocations (lower plate). The core regions have higher Ψ.[21] As in 2D,[14] these dislocations do not disappear even if the shearing is stopped. They can be metastable due to the Peierls potential arising from the discrete lattice structure.[22]

In the two phase case we prepared a coherent domain structure at $T=0.42$ with $\langle\psi\rangle=0$, where the cuboidal domains are harder than the percolating matrix.[8] We then applied cyclic shear defined by $\dot{\gamma}=10^{-3}$ for $0<t-nt_p<t_p/2$ and $\dot{\gamma}=-10^{-3}$ for $t_p/2<t-nt_p<t_p$ $(n=0,1,\cdots)$ with period $t_p=780$, as shown in Fig. 1. Since e_4 takes considerably large values (~0.1) near the interfaces, dislocation formation is triggered earlier than in the one phase case. From the second cycle, $\gamma\sim0.1$ and 0.3 even for $\langle\sigma_{xy}\rangle=0$, and $\langle\sigma_{xy}\rangle\sim-0.13$ even for $\gamma=0$. Figure 3 shows snapshots of e_4 and Ψ at the three points marked in Fig. 1. The dislocation loops form the boundaries of the slip planes extending into the soft regions, while their ends are trapped at the interfaces. Figure 4 shows 2D cross sections of $(u_x-\gamma y, u_y)$ and Ψ.

In plastic flow we define a regular elastic strain γ_{el} by $\langle\sigma_{xy}\rangle=\mu_3\sin(2\pi\gamma_{el})/2\pi$ in terms of the average stress. We then define the average defect energy density,

$$f_D(t)=\langle f_{el}\rangle(t)-\langle f_{el}\rangle(0)-\langle\Psi(\gamma_{el},0,0)\rangle, \qquad (9)$$

in the course of cyclic shear. The first term is the average elastic energy density at time t, the second term is that at t

$=0$ arising from the deformations around the domains ($=8\times10^{-4}\mu_{20}$), and the third term is the regular elastic energy density due to γ_{el}. As shown in Fig. 5, $f_D(t)$ is around $10^{-3}\mu_{20}$ for $\gamma\lesssim0.3$ from the second cycle. For larger γ, however, $f_D(t)$ increases abruptly with increasing γ, where the Peierls potential is broken and the dislocation loops begin to expand. If dislocations give rise to an elastic energy density of order $10^{-3}\mu_{20}$, the dislocation line density becomes of order $2\times10^{-3}/a^2$.[23] The same order of magnitude can also be obtained directly if the total length of high-value regions of Ψ is divided by the system volume (see Fig. 3).

In summary, developing a simple efficient scheme, we have studied dislocation dynamics in binary alloys under simple shear deformations. Their gliding motion along the Burgers vector[4] is preferentially into the softer regions. Therefore, the composition dependence of the elastic moduli in Eq. (6) (elastic inhomogeneity) is essential in our theory. Note that our simulation times are much shorter than the time scale of the composition evolution. As has been confirmed in our previous two-dimensional simulation,[13] there should eventually appear a compositional Cottrell atmosphere around each dislocation core also in three dimensions,[4] which can affect dislocation dynamics and phase separation on long time scales. We will examine in future how dislocations influence various phase transitions in solids. In addition, in one phase states, dislocations tend to be formed close to preexisting dislocations and shear bands, where strains are localized, thicken with decreasing the shear rate in the plastic flow.[20,24] Simulation of dislocation formation under uniaxial deformations is also under way.

This work was supported by Grants in Aid for Scientific Research and for the 21st Century COE project from the Ministry of Education, Culture, Sports, Science and Technology of Japan.

[1] J. L. Strudel, in *Physical Metallurgy*, edited by R. W. Cahn and P. Haasen (North-Holland, Amsterdam, 1996), p. 2106; A. S. Argon, *ibid.*, p. 1878; P. Haasen, *ibid.*, p. 2010.

[2] S. Iwamura and Y. Miura, Acta Mater. **52**, 591 (2004).

[3] T. M. Pollock and A. S. Argon, Acta Metall. Mater. **40**, 1 (1992).

[4] A. H. Cottrell, *Dislocations and Plastic Flow in Crystals* (Clarendon, Oxford, 1953).

[5] J. W. Cahn, Acta Metall. **9**, 795 (1961).

[6] A. G. Khachaturyan, *Theory of Structural Transformations in Solids* (Wiley, New York, 1983).

[7] P. Fratzl, O. Penrose, and J. L. Lebowitz, J. Stat. Phys. **95**, 1429 (1999).

[8] A. Onuki, *Phase Transition Dynamics* (Cambridge University Press, Cambridge, 2002); H. Nishimori and A. Onuki, J. Phys. Soc. Jpn. **60**, 1208 (1991); A. Onuki and A. Furukawa, Phys. Rev. Lett. **86**, 452 (2001).

[9] F. Léonard and R. C. Desai, Phys. Rev. B **58**, 8277 (1998).

[10] Y. Wang, D. J. Srolovitz, J. M. Rickman, and R. LeSar, Acta Mater. **48**, 2163 (2000).

[11] S. Y. Hu and L. Q. Chen, Acta Mater. **49**, 463 (2001); Comput. Mater. Sci. **23**, 270 (2002).

[12] Y. U. Wang, Y. M. Jin, A. M. Cuitiño, and A. G. Khachaturyan, Acta Mater. **49**, 1847 (2001).

[13] A. Minami and A. Onuki, Phys. Rev. B **70**, 184114 (2004).

[14] A. Onuki, Phys. Rev. E **68**, 061502 (2003).

[15] V. Bulatov, F. F. Abraham, L. Kubin, B. Devincre, and S. Yip, Nature (London) **391**, 669 (1998).

[16] M. J. Buehler, A. Hartmaier, H. Gao, M. Duchaineau, and F. F. Abraham, Comput. Methods Appl. Mech. Eng. **193**, 5257 (2004).

[17] A $\pi/2$ rotation around the y axis gives $e_2'=e_2/2+\sqrt{3}e_3/2$, $e_3'=\sqrt{3}e_2/2-e_3/2$, $e_4'=-e_5$, $e_5'=e_4$, and $e_6'=-e_6$. The rotation around the z axis reduces to that in 2D and is rather trivial (Ref. 13).

[18] In terms of the usual elastic moduli C_{11}, C_{12} and C_{44} we have $\mu_2=(C_{11}-C_{12})/2$ and $\mu_3=C_{44}$.

[19] More generally, we need to use the convective time derivative $\partial/\partial t+\boldsymbol{v}\cdot\nabla$ in Eqs. (7) and (8) for large strains.

[20] For $\dot{\gamma}=10^{-3}$ the separation of the slip planes has become 1.5 longer than for $\dot{\gamma}=10^{-4}$ in Fig. 2.

[21] Around dislocations produced by shear strain, Φ is typically 10% of Ψ.

[22] R. Peierls, Proc. Phys. Soc. London **52**, 34 (1940).

[23] The elastic energy of edge dislocations per unit length is $a^2\mu_{20}\ln(\ell/a)/4\pi(1-\nu)$ in isotropic elasticity, where ℓ is the distance among the dislocations and ν is the Poisson ratio. Then we obtain a rough estimation of the dislocation line density ($\sim\ell^{-2}$) in the text.

[24] Shear bands have been observed from nanometer scales to macroscopic scales particularly in metallic glasses. The dynamics of their growth is still not well understood.